Available online at www.sciencedirect.com

ScienceDirect

Procedia Structural Integrity 2 (2016) 2706–2717

Structural Integrity Procedia

www.elsevier.com/locate/procedia

21st European Conference on Fracture, ECF21, 20-24 June 2016, Catania, Italy

Multiaxial Fatigue Crack Propagation of an Edge Crack in a Cylindrical Specimen Undergoing Combined Tension-Torsion Loading

R.Citarella[a], R. Sepe[b]*, V. Giannella[a], I. Ishtyryakov[c]

[a]*Dept. of Industrial Engineering, University of Salerno, via G. Paolo II, 132 - 84084 Fisciano, Italy.*
[b]*Dept. of Industrial and Information Engineering, Second University of Naples, Via Roma, 29 - 81031 Aversa, Italy.*
[c]*Kazan Scientific Center of Russian Academy of Sciences, Lobachevsky Street, 2/31 - 420111 Kazan, Russia.*

Abstract

A three-dimensional crack propagation simulation of a hollow cylinder undergoing coupled traction and torsion loading conditions is performed by the Dual Boundary Element Method (DBEM). The maximum tension load and torque are equal to 40 kN and 250 Nm respectively. Specimens, made of Al alloys B95AT and D16T, have been experimentally tested with in-phase constant amplitude loads. The Stress Intensity Factors (SIFs) along the front of an initial part through crack, initiated from the external surface of the hollow cylinder, are calculated by the J-integral approach. The crack path is evaluated by using the Minimum Strain Energy Density (MSED) criterion whereas the Paris' law, calibrated for the material under analysis, is used to calculate crack growth rates. A cross comparison between DBEM and experimental results is presented, showing a good agreement in terms of crack growth rates and paths.

Peer-review under responsibility of the Scientific Committee of ECF21.

Keywords: DBEM; Mixed-Mode Crack propagation; Multiaxial fatigue.

1. Introduction

Numerical modeling of three-dimensional (3D) fatigue crack growth under mixed mode conditions represents a crucial factor in fracture mechanics in order to assess the residual life of components. The fatigue growth analysis of

* Corresponding author. Tel.:+39-081-501-03-18;
E-mail address: raffsepe@unina.it

Peer review under responsibility of the Scientific Committee of ECF21.
10.1016/j.prostr.2016.06.338

surface cracks is one of the most important elements for structural integrity prediction of the circular cylindrical metallic components (bars, wires, bolts, shafts, etc.), in the presence of initial and accumulated in service damages. In most cases, part-through flaws appear on the free surface of the cylinder and their shape generally assumes a semi-elliptical geometry. Multi-axial loading conditions, including tension/compression, bending and torsion are typical for the cylindrical metallic components of engineering structures. The problem of residual fatigue life prediction of such type of structural elements is complex and a closed solution is often not available because surface flaws are three-dimensional in nature.

In (Citarella et al., 2014; 2015), experimental and numerical results of fatigue crack growth for a crack initiated from a straight-fronted edge notch in an elastic bar under axial loading, with or without superimposed cyclic torsion, are given, and the influence of different loading conditions on fatigue life is discussed. The relations between crack opening displacement and crack length, measured on the free specimen surface, are obtained, so that the crack front shape and crack growth rate in the depth direction can be predicted. The numerical simulations in (Citarella et al., 2014) are based on the Dual Boundary Element Method (DBEM) whereas, the same calculations are performed in (Citarella et al., 2015) using the Finite Element Method (FEM). In the past, a comparison between FEM and DBEM results on this kind of problems was already attempted but separately considering the two loading conditions (Citarella et al., 2015; Citarella and Buchholz, 2008; Citarella and Cricrì, 2010). Now the comparison is extended in case of simultaneous application of the torsion and traction fatigue loads, considering a different material and a different specimens geometry than in (Citarella et al., 2014; 2015). In particular, in this work, a three-dimensional crack propagation simulation is performed by DBEM for a hollow cylinder undergoing coupled traction and torsion loading conditions. The maximum tension load and torque are equal to 40 kN and 250 N·m respectively.

Specimens have been experimentally tested with in-phase constant amplitude loads in order to provide data useful to validate the numerical procedure.

The Stress Intensity Factors (SIFs) along the front of an initial part through crack, initiated from the external surface of the hollow cylinder, are calculated by the J-integral approach (Dell'Erba and Aliabadi, 2001; Rigby and Aliabadi, 1993) rather than Crack Opening Displacement (COD) (Calì et al., 2003; Citarella and Perrella, 2005), being the former more accurate and less dependent on mesh refinement level. The computational 3D fracture analyses deliver variable mixed mode conditions along the crack front.

The crack path is evaluated by using the Minimum Strain Energy Density (MSED) criterion (Sih and Cha, 1974) whereas the crack growth rates are calculated by the Paris' law, calibrated for the material under analysis. In final, a cross comparison between DBEM and experimental results is presented, showing a good agreement in terms of crack growth rates and paths.

2. Experimental test

Specimen geometry is shown in Fig. 1: the depth of the initial curvilinear edge notch is denoted by h and the current crack depth by a, with the crack front approximated by an elliptical curve with characteristic sizes c and a. Using cutting machine, surface edge notches were cut with initial depths h = 3.0 mm for both circular arc and elliptical-arc initial shape. The crack length b is obtained by measuring the distance between the advancing crack break through point and the notch break through point along the free surface. The crack opening displacement is measured on the specimen cylindrical surface, in the central axial plane of symmetry, as shown in Fig. 2.

The Axial Torsion machine testing Bi-00-701 (Fig. 3) is used for axial-torsional fatigue and fracture testing of the hollow cylindrical specimens. This system is equipped with: fatigue rated axial-torsional dynamic load cell with axial capacity 100 kN and torsional capacity 2 kN·m and Bi-06-3XX series axial extensometers and torsional strain measurement fixture. The crack length on the specimen lateral surface was monitored using the optical instrumental zoom microscope whereas, to measure the crack opening displacement a pulley arrangement with an externally axial encoder is introduced (Fig. 3).

All tests are carried out with sinusoidal loading form, under load and torque control at frequency of 10 Hz. For the tension fatigue tests, the specimens are tested with an applied maximum nominal stress equal to σ = 65 MPa. The multiaxial tension/torsion tests are performed applying synchronous and in-phase tensile and shear stresses whose maximum values are respectively equal to σ = 75 MPa and τ = 59 MPa.

During tests, the stress ratio is modified from $R = 0.1$ to $R = 0.5$ (and reverse) in order to create beach marks on the fracture surface. As a matter of fact, the stress ratio increase from 0.1 to 0.5, at constant value of maximum cyclic nominal stress, produces beach marks that can be detected in a post mortem fractographic analysis; such stress ratio variation was applied when the surface crack length was approximately extended by $a \cong 0.1$mm.

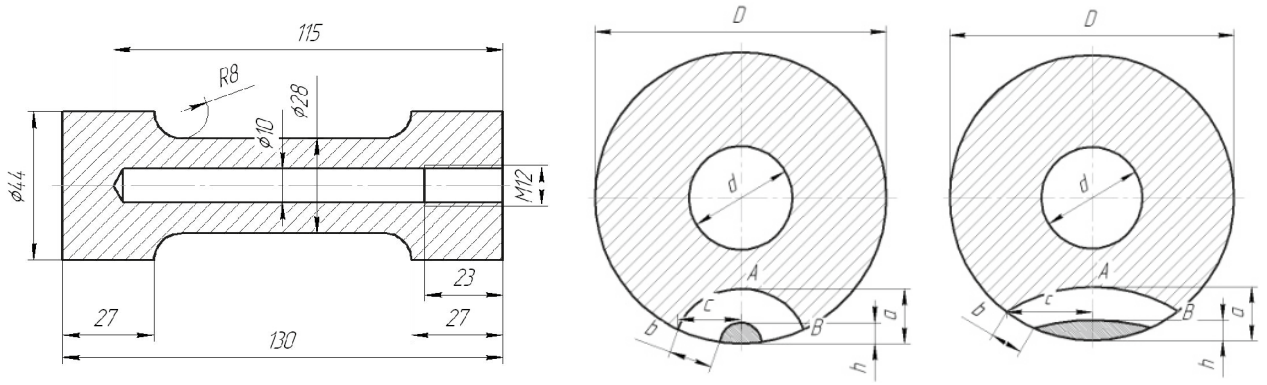

Fig. 1. Details of the hollow specimen geometry and initial notches.

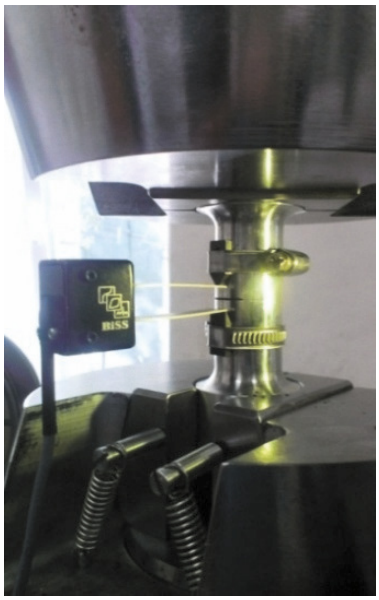

Fig. 2. Test equipment for measuring COD and edge crack current sizes.

Specimens are made of aluminium alloys D16T and B95AT whose main mechanical properties are listed in Table 1, where: E is the Young's modulus, σ_b is the nominal ultimate tensile strength, σ_{02} is the monotonic tensile yield strength, σ_u is the true ultimate tensile strength, δ is the elongation, ψ is the reduction of area, n is the strain hardening exponent and α is the strain hardening coefficient.

Table 1. Main mechanical properties of aluminum alloys.

Aluminum alloy	$\sigma_{0.2}$ [MPa]	σ_b [MPa]	δ [%]	ψ [%]	σ_u [MPa]	E [GPa]	n	α
D16T	437	643	14.97	11	665	80.636	5.86	1.54
B95AT	518	653	14	36	775	78.596	10.37	1.46

Fig. 3. Axial Torsion Test System Bi-00-701.

The typical beach marks on the post mortem cross section of different specimens are shown in Figs. 4 and 5 for tension and tension/torsion, respectively. From the crack front shape obtained in this way, the relations between the relative crack depth *a/D* and the surface crack chord length *c/D* can be measured using a comparison microscope. In addition, based on periodically measured increments of surface crack chord length *Δb*, the curve of surface crack propagation rate *db/dN* versus cycle number *N* can be obtained. Based on this, utilizing the relation of crack depth versus *Δb*, it is possible to obtain the crack growth rates *da/dN* along the depth direction.

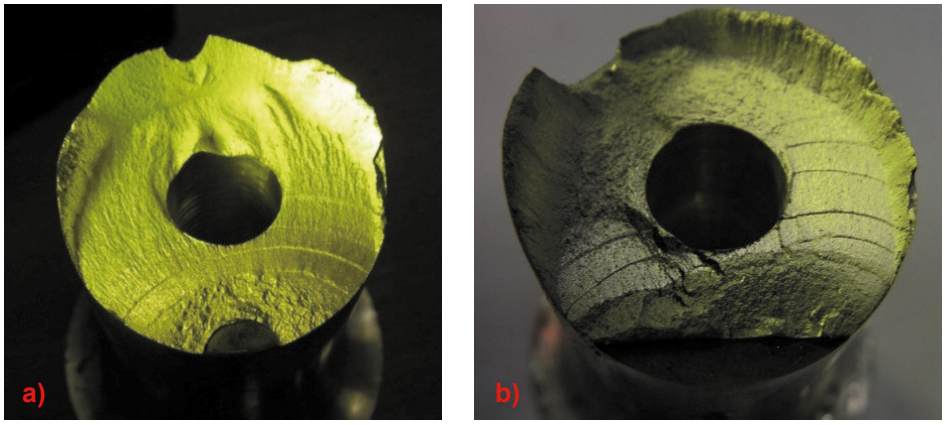

$a_0/c_0 = 0.9$ $a_0/c_0 = 0.37$

Fig. 4. Post mortem cross sections of specimen undergoing pure tension: a) circular notch; b) semielliptical notch.

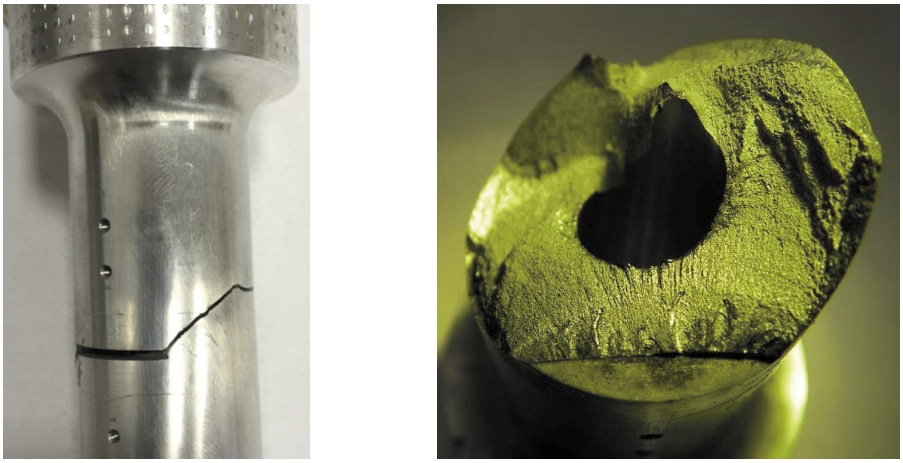

Fig. 5. Crack surface of specimen undergoing tension-torsion combined load.

Another interesting result pointed out in the present study is the crack front and aspect ratio stabilization (Fig. 6) with respect to different initial notch geometry, when considering the analyzed axial tension loading condition. It can be seen that the crack shape differ when diverse initial flaw forms are considered, but converge to the same configuration when the crack depth ratio *a/D* becomes larger than about 0.25.

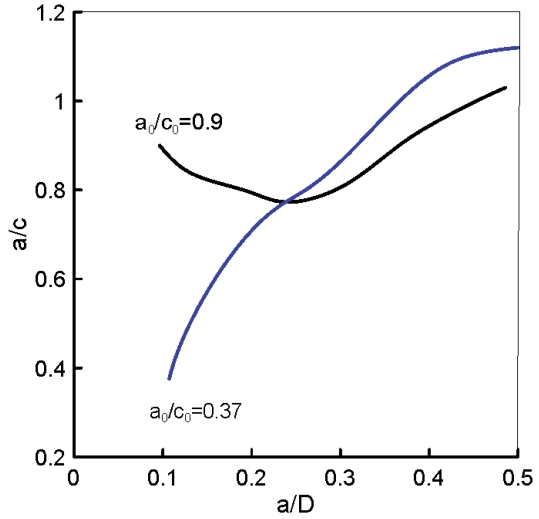

Fig. 6. Aspect ratio versus crack depth under tension for different initial surface flaw geometries.

3. Numerical analyses

Numerical simulations have been carried out by means of Dual Boundary Element Method (DBEM). SIFs are extracted from the J-integral using the equation:

$$J = \frac{1}{\overline{E}}\left(K_I^2 + K_{II}^2\right) + \frac{1}{2G}\left(K_{III}^2\right) \tag{1}$$

where: $\overline{E} = E/\left(1-\nu^2\right)$ for plain strain conditions.

3.1. Specimen undergoing pure tension load

The cylindrical specimen (Fig. 7) has been modeled by BEASY (Beasy, 2011) using 1460 quadratic elements. The whole bottom surface has been constrained along three directions, whereas, top surface has been loaded with axial tractions with a resultant magnitude equal to 35 kN. In addition, constraints along tangential and radial directions have been applied on some elements (as shown in Fig. 7) in order to guarantee a pure axial translation and correctly reproduce the experimental loading conditions.

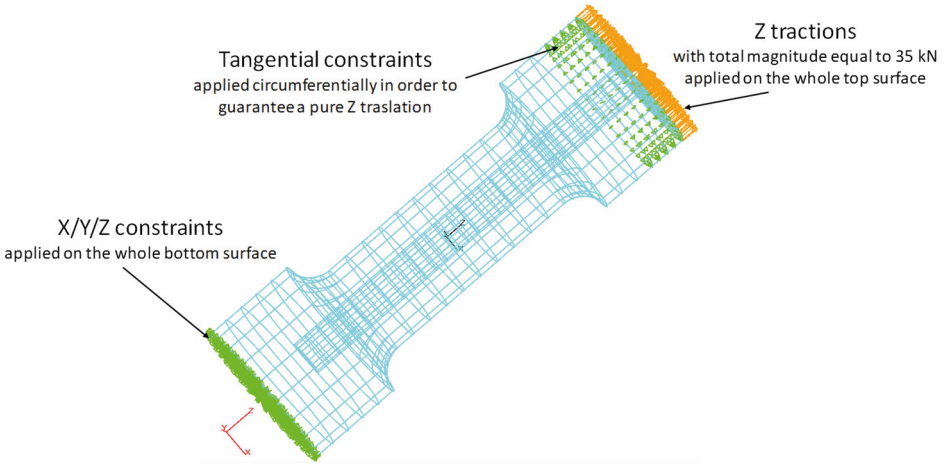

Fig. 7. Boundary conditions applied on the DBEM model for specimen under tension loading.

Two different initial cracks have been modeled and introduced in the DBEM model as illustrated in Fig. 8, in which crack size definitions are detailed. They are not available in the crack database, where just “standard” crack shapes are provided, so were manually created and added in the DBEM domain; then J-paths (rings of internal points in which J-integral calculations are performed) are positioned along crack front and the remeshing phase of the crack surrounding area is automatically performed. After crack insertion, the number of elements increases to 2316 and 3509, for the cracks associated with the circular and semi-elliptical notch respectively.

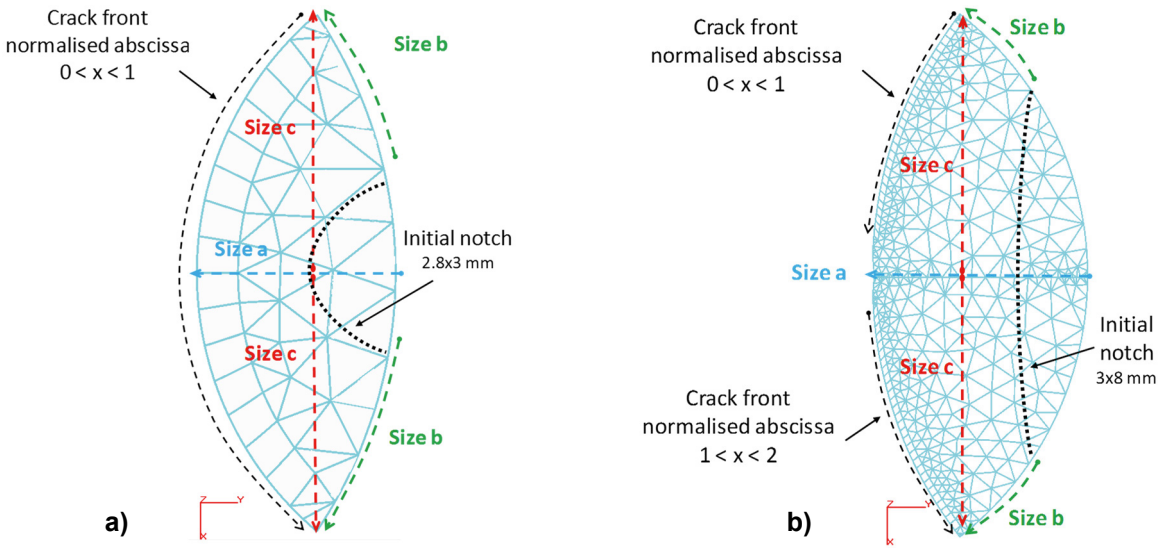

Fig. 8. DBEM initial crack geometry with size definitions: a) circular notch; b) semielliptical notch.

3.2. Specimen under combined tension/torsion loading

The specimen undergoing tension and torsion loads is modeled using the same DBEM model previously described. Tangential constraints are substituted by tangential tractions with a resultant magnitude equal to 250 Nm whereas radial constraints are kept in order to guarantee a pure Z translation and axial rotation (Fig. 9). The resultant traction applied load is equal to 40 kN.
Then, a 3D crack has been modeled, representing the initial crack scenario coming out from considering the semielliptical notch; the corresponding number of elements is equal to 4905 (Fig. 10).

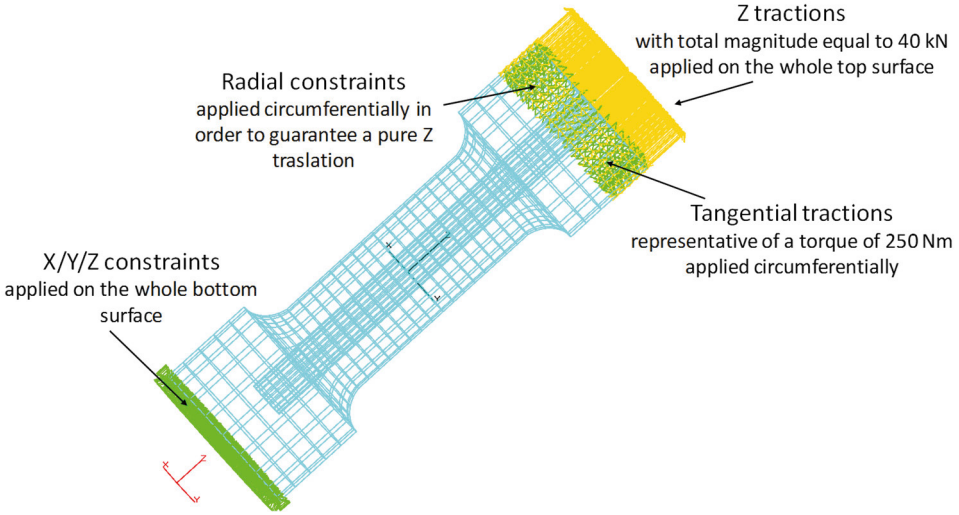

Fig. 9. Boundary conditions applied on the DBEM uncracked model for specimen under tension/torsion loading.

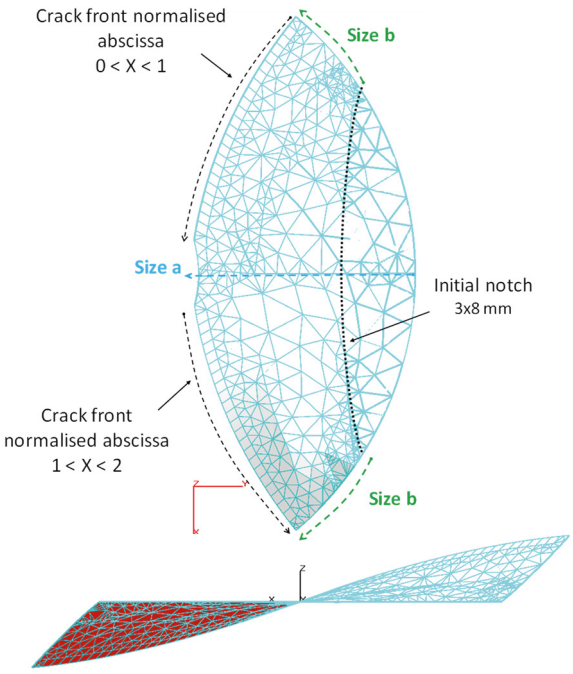

Fig. 10. Initial crack with size definitions (up) and final kinked crack (down) for specimen under multiaxial loading.

4. Results

4.1. Specimen undergoing pure traction load

The cracked DBEM models related to the initial circular or semielliptical notch have been solved and the related von Mises stress scenarios are shown in Fig. 11.

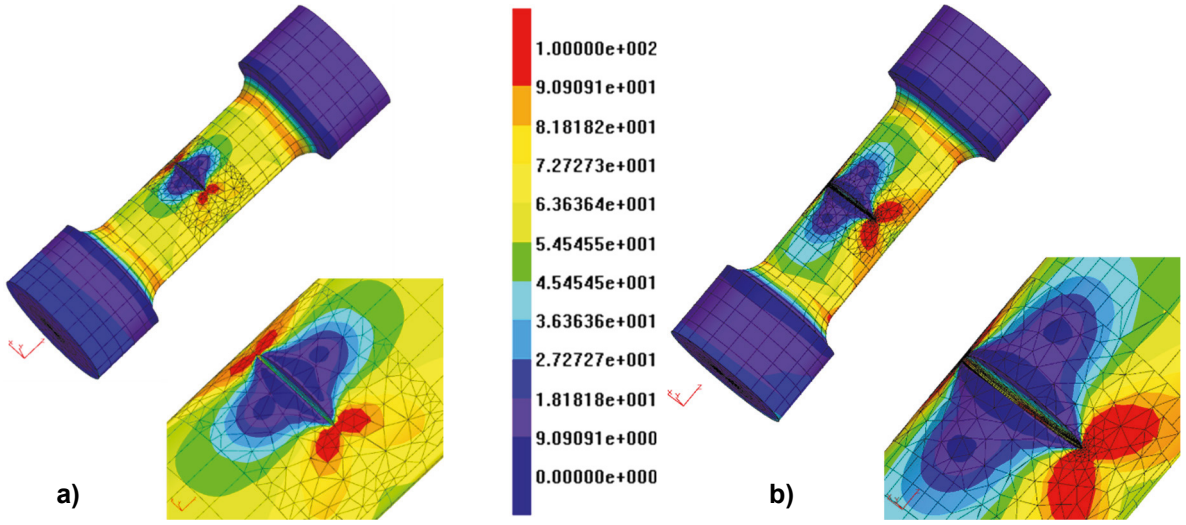

Fig. 11. Von Mises stress scenario (MPa) for the initial cracked configurations: (a) circular notch; (b) semielliptical notch.

Then, two crack propagations have been simulated using the Paris' law (calibrated for the material under analysis). Kink angles have been calculated using the Minimum Strain Energy Density (MSED) criterion and SIFs are computed by means of J-integral.

The stress fields related to the final crack scenarios are shown in Fig. 12 whereas in Fig. 13 it is possible to appreciate the similarities between numerical and experimental crack fronts.

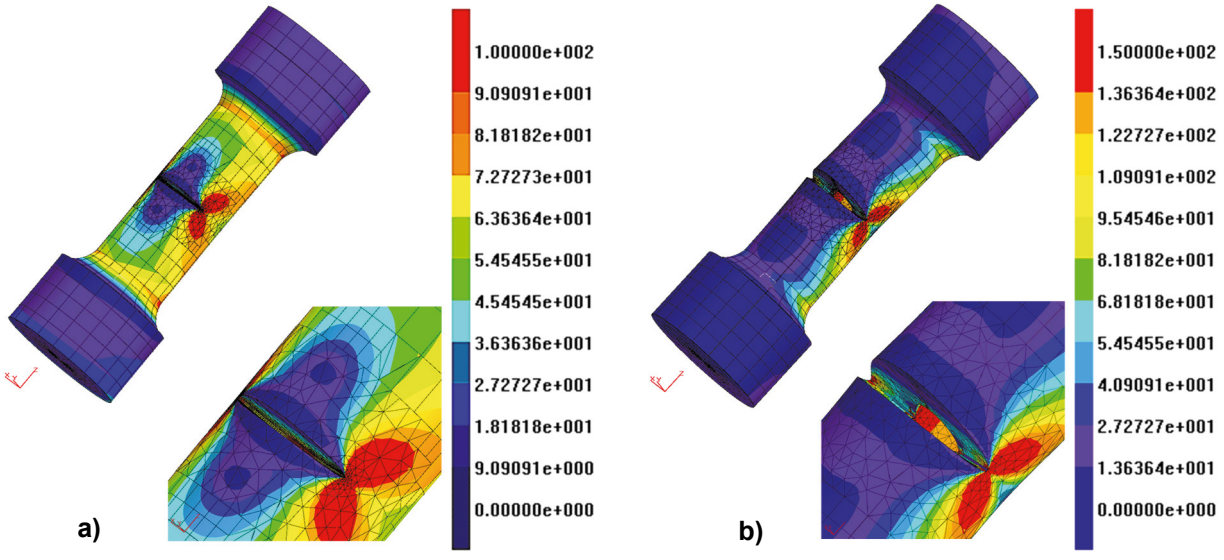

Fig. 12. Von Mises stress (MPa) scenario for the final cracked configuration: (a) circular notch; (b) semielliptical notch.

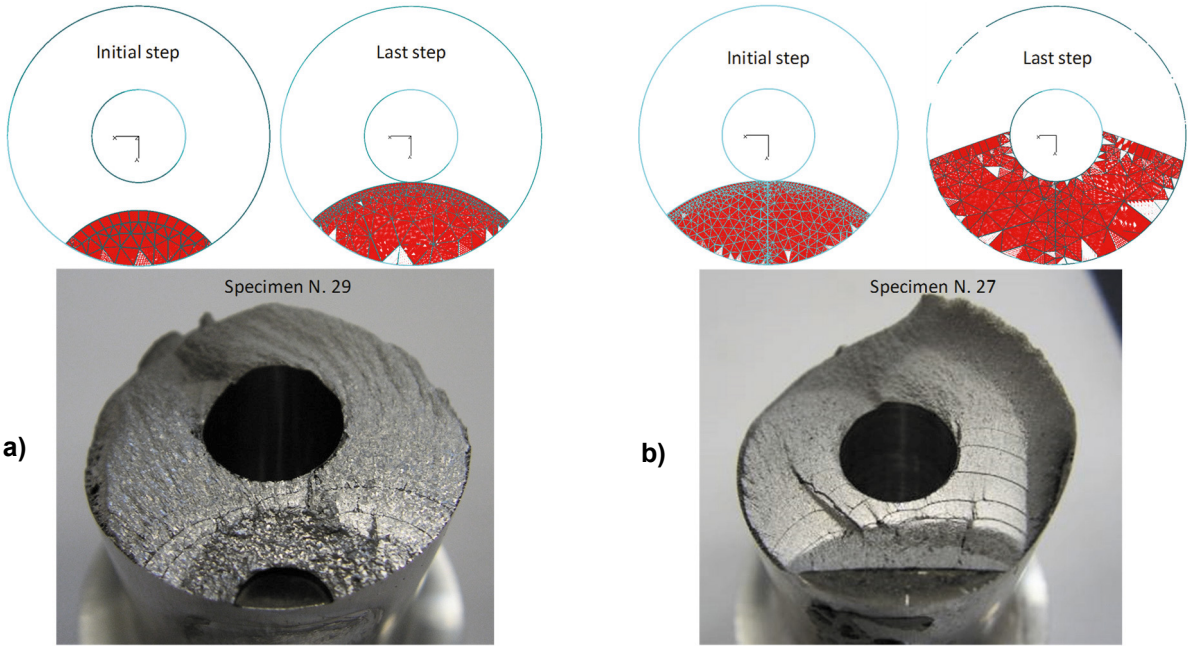

Fig. 13. Numerical initial and final crack shapes vs. beach marks highlighting the experimental crack fronts: (a) circular notch; (b) semielliptical notch.

K_I values along crack front for different propagation steps are plotted in Fig. 14: Fig. 14a shows K_I values calculated for the configuration related to the circular notch, whereas, Fig. 14b shows K_I values related to the semielliptical notch (the crack propagates under pure mode I conditions so that K_{II} and K_{III} values are negligibles).

In final, crack sizes calculated with DBEM analyses are plotted in Fig. 15 and compared with those obtained by the experimental tests.

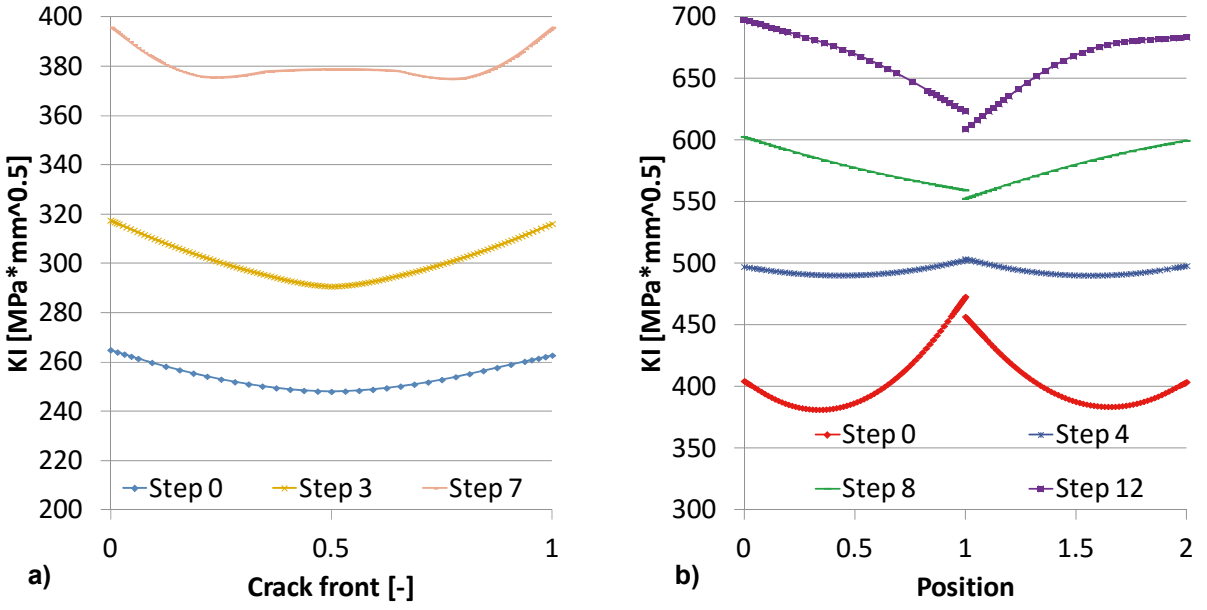

Figure 14. K_I values along crack front at several steps during propagation for tensile load: (a) circular notch; (b) semielliptical notch.

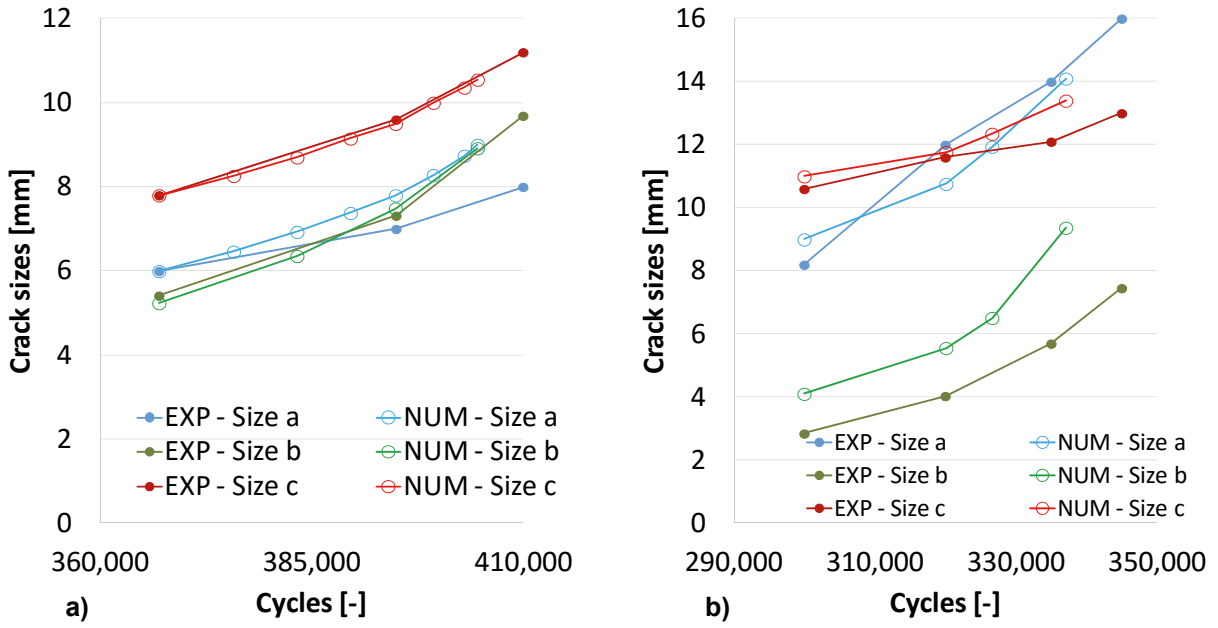

Fig. 15. Crack sizes comparison between experimental tests and DBEM analyses: (a) circular notch; (b) semielliptical notch.

4.2. Specimen undergoing tension/torsion loading

The DBEM model undergoing tensile and torsion loads, after the crack insertion, has been solved and crack propagation automatically performed; von Mises stresses are plotted for the initial and final crack configurations in Fig. 16, whereas a comparison between numerical and experimental crack shapes is shown in Fig. 17. Fig. 18 shows K_I, K_{II}, K_{III} values along crack front at several steps during the growth, whereas, a cross comparison between experimental test and numerical results is shown in Fig. 19 with reference to crack size vs. cycles.

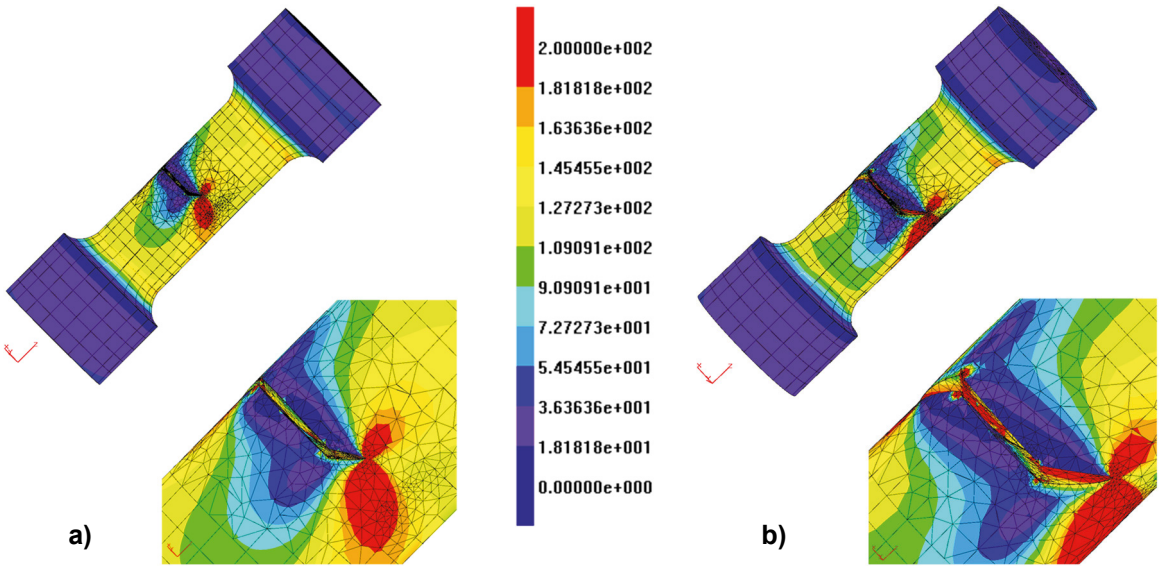

Fig. 16. Von Mises stress scenario (MPa) for the initial (a) and final (b) cracked configuration for model undergoing tension/torsion loads.

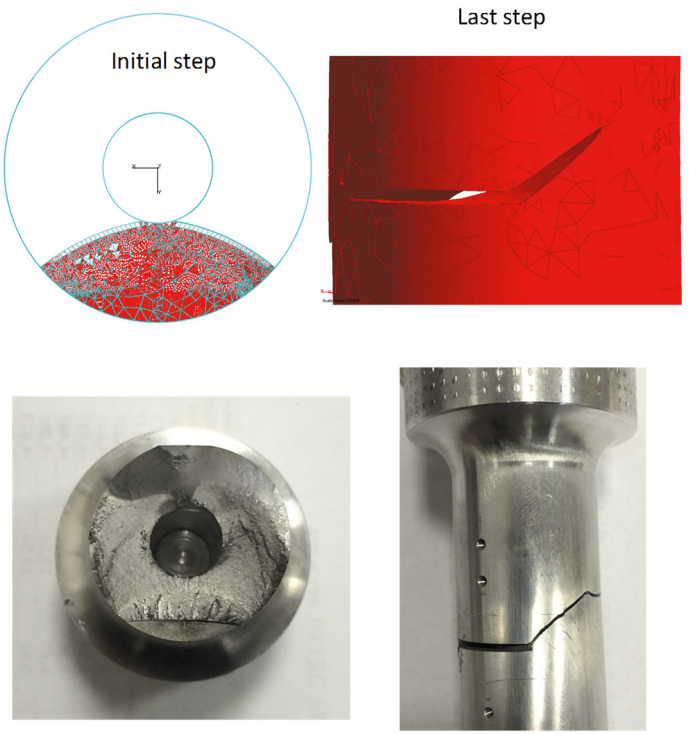

Figure 17. Numerical-experimental crack shape comparison for the specimen undergoing tension/torsion loads.

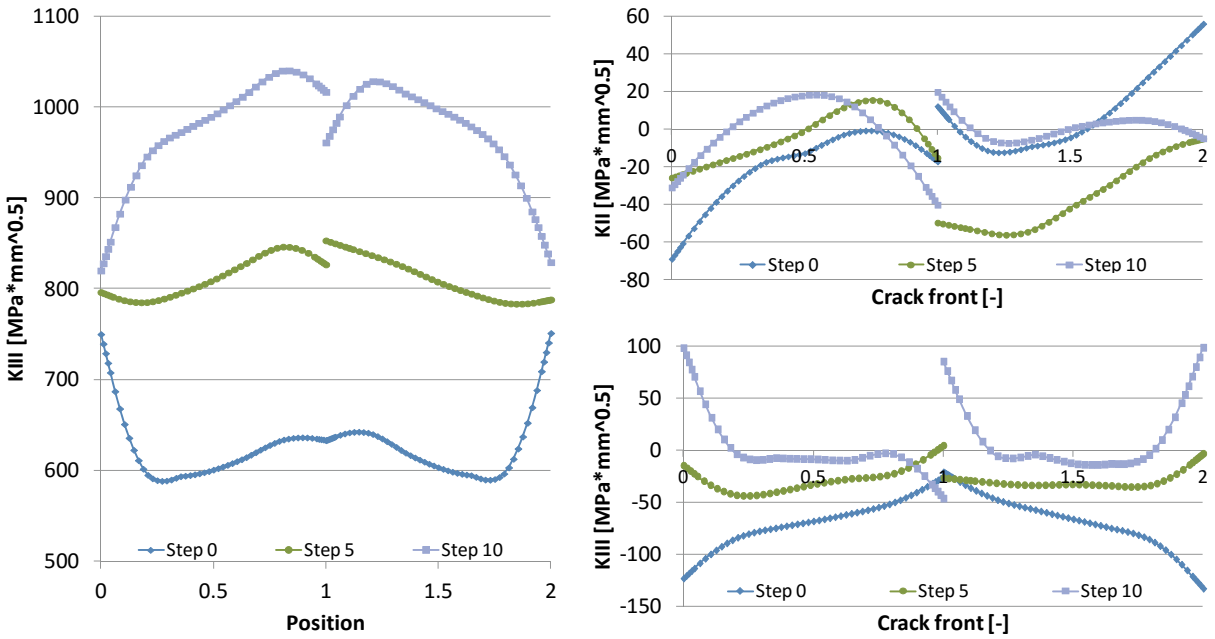

Figure 18. SIF values during growth for the configuration undergoing tension/torsion loads.

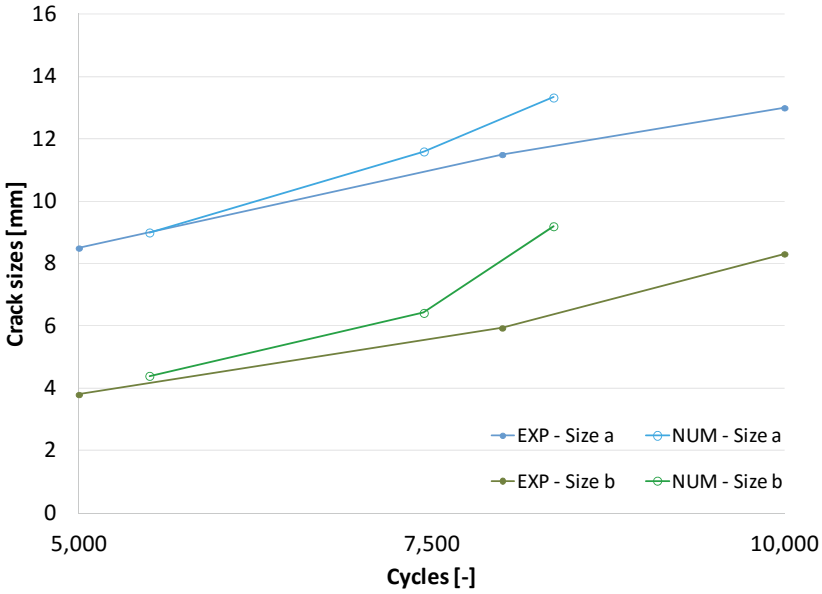

Figure 19. Crack sizes comparison between DBEM and experimental tests for the configuration undergoing tension/torsion loads.

5. Conclusion

The computed DBEM crack propagation results are found to be in good agreement with experimental findings in terms of crack growth rates. A rather complex 3D crack growth behavior is present in case of superimposed tension and in phase torsion and the fatigue life is decreased if compared to a pure tension fatigue load. This can be put in relation to the increase of the mode mixed effect. The crack insertion and the whole crack propagation is fully automatic, with repeated remeshing realized at each crack step without user intervention. Consequently, for the cases analyzed, the functionality of the proposed procedure can be stated.

References

BEASY V10r16. Documentation. C.M. BEASY Ltd., (2011).

Calì, C., Citarella, R., Perrella, M., 2003. Three-dimensional crack growth: numerical evaluations and experimental tests, European Structural Integrity Society 31 3-504, Biaxial/Multiaxial Fatigue and Fracture, Edited by Andrea Carpinteri, Manuel de Freitas and Andrea Spagnoli.

Citarella, R., Perrella, M., 2005. Multiple surface crack propagation: numerical simulations and experimental tests, Fatigue and Fracture of Engineering Material and Structures 28, 135-148.

Citarella, R., Buchholz, F.G., 2008. Comparison of crack growth simulation by DBEM and FEM for SEN-specimens undergoing torsion or bending loading. Engineering Fracture Mechanics 75, 489–509.

Citarella, R., Cricrì, G., 2010. Comparison of DBEM and FEM Crack Path Predictions in a notched Shaft under Torsion. Engineering Fracture Mechanics 77, 1730–1749.

Citarella, R., Lepore, M., Shlyannikov, V., Yarullin, R., 2014. Fatigue surface crack growth in cylindrical specimen under combined loading. Engineering Fracture Mechanics 131, 439–453.

Citarella, R., Lepore, M., Maligno, A., Shlyannikov, V., 2015. FEM simulation of a crack propagation in a round bar under combined tension and torsion fatigue loading. Frattura ed Integrità Strutturale 31, 138–147.

Citarella, R., Giannella, V., Lepore, M., 2015. DBEM crack propagation for nonlinear fracture problems. Frattura ed Integrità Strutturale 34, 514–523.

Dell'Erba, D.N., Aliabadi, M.H. 2001. DBEM analysis of fracture problems in three dimensional thermoelasticity using J-integral. Int J Solids Struct, 38(26–27), 4609–4630.

Rigby, R.H., Aliabadi, M.H., 1993. Mixed-mode J-integral method for analysis of 3D fracture problems using DBEM. Eng Anal Bound Elem 11, 239–256.

Sih, G.C., Cha, B.C.K., 1974. A fracture criterion for three-dimensional crack problems. Engineering Fracture Mechanics 6, 699–732.